Neural Networks 142 (2021) 44–56

Contents lists available at ScienceDirect

Neural Networks

journal homepage: www.elsevier.com/locate/neunet

Growth strategy determines the memory and structural properties of brain networks

Ana P. Millán [a,*], Joaquín J. Torres [b], Samuel Johnson [c,d], J. Marro [b]

[a] Amsterdam UMC, Vrije Universiteit Amsterdam, Department of Clinical Neurophysiology and MEG Center, Amsterdam Neuroscience, De Boelelaan 1117, Amsterdam, The Netherlands
[b] Institute 'Carlos I' for Theoretical and Computational Physics, University of Granada, Spain
[c] School of Mathematics, University of Birmingham, Edgbaston B15 2TT, UK
[d] Alan Turing Institute, London NW1 2DB, UK

ARTICLE INFO

Article history:
Received 19 October 2020
Received in revised form 4 March 2021
Accepted 20 April 2021
Available online 26 April 2021

Keywords:
Brain development
Co-evolving neural network
Associative memory
Complex networks
Temporal networks

ABSTRACT

The interplay between structure and function affects the emerging properties of many natural systems. Here we use an adaptive neural network model that couples activity and topological dynamics and reproduces the experimental temporal profiles of synaptic density observed in the brain. We prove that the existence of a transient period of relatively high synaptic connectivity is critical for the development of the system under noise circumstances, such that the resulting network can recover stored memories. Moreover, we show that intermediate synaptic densities provide optimal developmental paths with minimum energy consumption, and that ultimately it is the transient heterogeneity in the network that determines its evolution. These results could explain why the pruning curves observed in actual brain areas present their characteristic temporal profiles and they also suggest new design strategies to build biologically inspired neural networks with particular information processing capabilities.

1. Introduction

Complex networks are ubiquitous in nature: almost every biological and social system, as well as many man-made structures, develop intricate relations among its components, resulting in a network configuration that is usually far from being homogeneous (Barabási & Albert, 1999; Boccaletti, Latora, Moreno, Chavez, & Hwang, 2006; Newman, 2018). Research on complex networks has received a tremendous amount of attention over recent decades, in order both to understand natural networks and to optimize technical designs. Most studied networks have thus been shown to present non-trivial topological features, such as high clustering and short minimum paths (small-worldness), modular structure, and cost-efficient wiring (Albert, 2005; Eguíluz, Chialvo, Cecchi, Baliki, & Apkarian, 2005; Gastner & Ódor, 2016). Recurrent common properties are also a highly heterogeneous degree distribution (where the degree of a node is its number of neighbours) and, often, negative degree–degree correlations — a property known as disassortativity (Johnson, Torres, Marro, & Muñoz, 2011; Ódor, 2013; Piraveenan, Prokopenko, & Zomaya, 2008). In other words, many networks of interest include a small number of highly connected nodes, called hubs, which tend to be connected to low-degree nodes (Achard, Salvador, Whitcher, Suckling, & Bullmore, 2006; Crossley et al., 2014; Newman, 2003). These structural properties influence the emerging dynamics on the network. For instance, degree heterogeneity and degree–degree correlations strongly influence the signal to noise ratio in certain dynamical systems (de Franciscis, Johnson, & Torres, 2011; Marro & Torres, 2021; Maslov & Sneppen, 2002; Ódor & Hartmann, 2018; Schmidt, LaFleur, de Reus, van den Berg, & van den Heuvel, 2015; Torres, Muñoz, Marro, & Garrido, 2004), and the synchronization and diffusive properties of a complex network strongly depend on its dimensionality (Millán, Gori, Battiston, Enss, & Defenu, 2021; Millán, Torres and Bianconi, 2018, 2019), to name a few examples (Barrat, Barthelemy, & Vespignani, 2008).

In order to understand how such non-trivial networked structures come about, much work has gone into investigating mechanisms of network evolution. Models in which networks are gradually formed, for instance by the addition and/or deletion of nodes and links, or by the rewiring of the latter, have been studied in various contexts (Barabási & Albert, 1999; Berg, Lässig, & Wagner, 2004; Bianconi & Rahmede, 2016; Johnson, Torres, & Marro, 2009; Navlakha, Barth, & Bar-Joseph, 2015). Certain evolution rules have thus been shown to generate network topologies with particular properties, such as small-world, scale-free, or hierarchical-modular structures (Barabási & Albert, 1999; Bianconi, Darst, Iacovacci, & Fortunato, 2014; Bianconi & Rahmede,

* Corresponding author.
E-mail address: a.p.millanvidal@amsterdamumc.nl (A.P. Millán).

https://doi.org/10.1016/j.neunet.2021.04.027

2016; Millán et al., 2021; Watts & Strogatz, 1998). These rules often give rise to phase transitions, such that qualitatively different kinds of network topologies can ensue depending on parameters (Albert, 2005; Newman, 2003). In most studied networks the evolution of the topology is invariably linked to the state of the network and vice versa (Gross & Blasius, 2007), which has given rise to a novel field of study: *adaptive* or *co-evolving networks* (Sayama et al., 2013). The coupling between form and function creates a feedback loop between dynamics and topology, and yields some interesting dynamic phenomena, such as the formation of complex topologies, robust dynamical self-organization, and spontaneous emergence of different classes of nodes (Su, Ruan, Guan, & Liu, 2013; Vazquez, Eguíluz, & San Miguel, 2008; Wiedermann, Donges, Heitzig, Lucht, & Kurths, 2015).

Co-evolving models can be naturally applied to study brain development. The mammalian brain is initially formed through an initial rapid proliferation of synapses. Synaptic density thus reaches a peak during early infancy and from then on it begins a steady decline down to about half this value later in life, in a process known as *synaptic pruning* (Chechik, Meilijson, & Ruppin, 1998; Iglesias, Eriksson, Grize, Tomassini, & Villa, 2005). It is believed that the reason for reducing synaptic density is becoming more energetically efficient (Chechik, Meilijson, & Ruppin, 1999; Stepanyants, Hof, & Chklovskii, 2002). But then a question arises, why not begin life with the optimal synaptic density? Recent studies have suggested that details of synaptic pruning may have large implications on high-level brain functions, and they have been related to the emergence of some neurological disorders such as autism and schizophrenia (Faludi & Mirnics, 2011; Sayama et al., 2014). Similarly, a high synaptic density during infancy would allow for faster learning during this critical period (Knoblauch, 2017; Knoblauch, Körner, Körner, & Sommer, 2014; Knoblauch & Sommer, 2016). However, little is so far known about the influence of particular pruning profiles – describing the change in synaptic density over time – on cognitive development.

Here we consider a computational model of synaptic pruning that includes an initial transient period of high synaptic density, and may thus serve to analyse what factors affect both pruning efficacy and the structural and memory properties of the developed network. Our model adapts a biologically inspired co-evolving neural network model (Millán, Torres, Johnson and Marro, 2018; Millán, Torres and Marro, 2019) in which a feedback loop emerges between structure and dynamics, leading to two qualitatively different kinds of behaviours (Millán, Torres, Johnson et al., 2018; Millán, Torres, Marro, 2019): the network structure can become heterogeneous and disassortative, and display good memory stability, or the structure may remain homogeneous and incapable of memory retrieval. Here we show that the inclusion of an initial, transient period of relatively high synaptic density, even in a simple case, introduces a dependence of the evolution of the system on the initial synaptic density. This can, under certain circumstances, lead towards an increased memory stability, even in the presence of high levels of noise. Since our co-evolving system couples neuronal dynamics and network development, memory stability strongly depends on the features of the developing network and mainly on its level of heterogeneity. Moreover, we show that this mechanism is robust with respect to some of the details of the model. The basic mechanism which illustrates our model here need not be restricted to neural networks, but may help understanding how other structures form. For instance, protein interaction networks also change in evolutionary time scales in a way that is related to their physiological activity (Berg et al., 2004). In fact, as is the case of our model, most biological networks change with time so that pruning may be a general mechanism for network optimization trying to minimize energy consumption in an environment of limited resources without the need for a great amount of information specifying the initial topology. Moreover, this optimization strategy could also be of use for technical applications, allowing, e.g., the design of particular network architectures of artificial neural networks that are optimal for the realization of particular tasks.

2. Synaptic pruning model

In this work we make use of a previously defined mathematical framework to describe synaptic pruning (Johnson, Torres, Marro and Muñoz, 2010; Millán, Torres, Johnson et al., 2018). The model defines an evolving network on top of which a neuronal activity model runs. This model was previously shown to reproduce several aspects of brain networks, including a realistic pruning profile during development (Huttenlocher & Dabholkar, 1997; Johnson, Marro and Torres, 2010; Millán, Torres, Johnson et al., 2018; Navlakha et al., 2015) and a realistic scale-free degree distribution with an exponent between -2 and -3, as commonly observed experimentally (Eguíluz et al., 2005; Gastner & Ódor, 2016), with the emergence of hubs (Crossley et al., 2014; Stam, 2010). As we describe in detail below, the network backbone intrinsically affects neuronal dynamics through the structure of connections. In turn, the evolution of the network depends also on the activity state of the neurons through the synaptic currents. In this way, we define a co-evolving model in which the network structure (or form) and the neuronal activity (or function) are coupled.

Overall, the system consists of an undirected N-node network whose links change at discrete times. The neuronal model consists of an autoassociative Amari–Hopfield model (Amit, 1989), whereas network evolution is characterized by a preferential attachment mechanism (Johnson, Marro et al., 2010; Millán, Torres, Johnson et al., 2018; Millán, Torres, Marro, 2019). There is an implicit separation of time-scales in the model as node dynamics is considered to be much faster than link dynamics. In this manner, the network backbone is fixed during neuronal dynamics. In the following, we refer with t to the time-scale of link dynamics, and with τ to the time-scale of neuronal activity, in between link changes.

At time t, the adjacency matrix is $\{e_{ij}(t)\}$, $i,j = 1,\dots,N$, $e_{ii}(t) = 0$, $\forall t$, with element 1 or 0 according to whether there exists or not a link between the pair of nodes (i,j), respectively. The *degree* of node i at time t, indicating its number of links (and thus neighbouring nodes), is $k_i(t) = \sum_j^N e_{ij}(t)$, and the mean degree of the network – or *connectivity* – is

$$\kappa(t) = N^{-1}\sum_{i}^{N} k_i(t). \tag{1}$$

$\kappa(t)$ thus indicates the average number of links per node in the network. Given that the network is undirected, $\kappa(t)N = \sum_{i=1}^{N}\sum_{j=1}^{N} e_{ij}(t)$ is twice the total number of links (or synapses) in the network. The *synaptic density* is thus $\rho(t) \equiv \kappa(t)N/(2V)$, with V the total volume considered (Johnson, Marro et al., 2010). We define $\kappa_\infty = \kappa(t \to \infty)$ as the mean degree of the network in the stationary limit.

2.1. Neuronal activity model

Neuronal dynamics is defined following the canonical definition of the Amari–Hopfield model and Hebbian synapses, in line with a large number of previous studies (Amari, 1972; Amit, 1989; de Franciscis et al., 2011; Hebb, 2005; Hopfield, 1982; Morelli, Abramson, & Kuperman, 2004; Recio & Torres, 2016; Torres et al., 2004; Uhlig, Levina, Geisel, & Herrmann, 2013), as

a standard way to define auto-associative neural networks. Each neuron i is modelled by a stochastic binary variable $s_i(t,\tau) = \{0,1\}$, indicating a silent or firing neuron, respectively. Similarly, each link or synapse is characterized by its synaptic weight w_{ij}. These are set (at $t = 0$) to encode a *memory or activity pattern* specifying a particular state of each of the neurons in the network, s_i^P. The pattern is made to be the attractor of the activity dynamics by an appropriate definition of the *synaptic weights*, according to the Hebbian learning rule (Amit, 1989; Bi & Poo, 2001; Hebb, 2005),

$$w_{ij} = \frac{1}{\kappa_\infty a_0(1-a_0)}(s_i^P - a_0)(s_j^P - a_0), \tag{2}$$

where $a_0 = \langle s_i^P \rangle$ is the mean activation of the pattern. In agreement with previous studies, we consider here the case $a_0 = 0.5$ (Millán, Torres, Johnson et al., 2018; Millán, Torres, Marro, 2019).

The neuronal states $s_i(t,\tau)$ follow an Amari–Hopfield dynamics, such that the neuron's probability of being on the active state at time $\tau + 1$ is given by

$$P\{s_i(t,\tau+1) = 1\} = \frac{1}{2}\left[1 + \tanh\left(T^{-1}\left[h_i(t,\tau) - \theta_i(t)\right]\right)\right], \tag{3}$$

where T is a noise parameter – or *temperature* – setting the level of noise in the neuron response, such that $T = 0$ corresponds to the deterministic limit (Amit, 1989; Bortz, Kalos, & Lebowitz, 1975). $h_i(\tau)$ is the *local field* at neuron i,

$$h_i(t,\tau) = \sum_{j=1}^{N} w_{ij} e_{ij}(t) s_j(\tau), \tag{4}$$

and $\theta_i(t)$ the neuron's *threshold* setting the excitability in the model,

$$\theta_i(t) = \frac{1}{2}\sum_{j=1}^{N} w_{ij} e_{ij}(t), \tag{5}$$

Both h_i and θ_i depend on the network structure through the adjacency matrix $e_{ij}(t)$. For the sake of simplicity, in the following we define

$$I_i(t,\tau) = \left|h_i(t,\tau) - \theta_i(t)\right|, \tag{6}$$

i.e.

$$I_i(t,\tau) = \left|\sum_{j=1}^{N} w_{ij} e_{ij}(t)\left[s_j(\tau) - \frac{1}{2}\right]\right|, \tag{7}$$

as the incoming current at each neuron from its neighbours. Thus, Eq. (3) becomes

$$P\{s_i(t,\tau+1) = 1\} = \frac{1}{2}\left[1 + \tanh\left(T^{-1} I_i(t,\tau)\right)\right], \tag{8}$$

Note that the previous definitions assure that all nodes (both silent ($s_i = 0$) and active ($s_1 = 1$) ones) take part in the memory state, as they are all considered in the definition of the synaptic weights (Eq. (3)) and local current (Eq. (8)). Moreover, the inclusion of a_0 in Eqs. (3) and (5) assures that there is a symmetry between active and inactive states. These definitions are typically considered within the Amari–Hopfield model when the more biologically plausible 0, 1 coding is used to define the neuronal states, instead of the canonical $-1, +1$ one, since it allows one to recover the phase diagram of the canonical, fully connected Amari–Hopfield model (Amit, 1989). In our context, $\theta_i(t)$ depends only on the existing synapses, which can be seen as a means of homeostasis since the response of a neuron is regulated by the number and strength of its synaptic contacts, thus avoiding silencing low-degree neurons and saturation of hubs. Furthermore, $\theta_i(t)$ depends indirectly on the neural activity through the term $e_{ij}(t)w_{ij}$ – which also characterizes the intensity of the synaptic transmission between neurons i and j.

Within this framework, the macroscopic activity state of the network can be measured via its *overlap* with the memorized (or encoded) pattern, that is,

$$m(t,\tau) = \frac{1}{Na_0(1-a_0)}\sum_{j=1}^{N}(s_i^P - a_0)s_i(t,\tau), \tag{9}$$

with $m \in [-1, 1]$. The overlap as seen by the pruning dynamics is $m(t) = m(t, \tau = h_s)$. m measures the resemblance of the current network state with the memorized activity pattern. Thus, $m \to 1$ implies that the neuronal state of the system is highly similar to the stored pattern, in which case we say that the system is in a *memory state*. On the contrary, $m \to 0$ indicates that the neuronal state does not resemble the stored pattern, i.e. the system is in a noisy state. Note that, due to the underlying symmetry, the anti-pattern (all nodes in the opposite state relative to the pattern) is also a stable attractor, and $m \to -1$ also indicates a memory state (Amit, 1989). Thus, we define the *stationary overlap* as $\tilde{m} \equiv |m(t \to \infty)|$ to account for this symmetry.

The canonical Amari–Hopfield model, which is here a reference, is defined on a fully connected network ($e_{ij} = 1,\ \forall i = j$). In this case, $\tilde{m}$ undergoes a continuous transition as a function of the noise level T, with a critical point at $T_c = 1$. The transition is from a ferromagnetic phase in which memory recovery is possible ($\tilde{m} \to 1$) and the system displays associative memory, for $T < 1$, to a paramagnetic one dominated by noise ($\tilde{m} \approx 0$) in which the system does not display associative memory, for $T > 1$. However, variations of different network characteristics, such as the mean degree or the degree–degree correlations can affect the location and nature of the transition (Amit, 1989; de Franciscis et al., 2011; Morelli et al., 2004; Uhlig et al., 2013).

The overlap parameter is a standard way to measure memory in attractor neural networks, and it has been commonly used in previous analysis on the Amari–Hopfield model (Amit, 1989; de Franciscis et al., 2011; Hebb, 2005; Millán, Torres, Johnson et al., 2018; Millán, Torres, Marro, 2019; Morelli et al., 2004; Recio & Torres, 2016; Torres et al., 2004; Uhlig et al., 2013). Given that all nodes take part in the memory state (both active and silent), they are all taken into account in Eq. (9). The overlap indicates the memory state regardless of the number of memorized patterns and their mean activity a_0. Other common metrics, such as the *mean firing rate*, provide no direct information within our current formulation, given that both the memory and noisy states have mean firing rate of 0.5.

2.2. Neural network development

The topology of the neural network changes in time following a Markov process given by the probabilities $P_i^g(t)$ and $P_i^l(t)$ that each node i has to be selected to gain and lose a link at time t, respectively. These are assumed to factorize in two terms, a global and a local one, namely

$$\begin{aligned} P_i^g(t) &= u\left[\kappa(t)\right]\ \pi\left[I_i(t)\right] \\ P_i^l(t) &= d\left[\kappa(t)\right]\ \eta\left[I_i(t)\right]. \end{aligned} \tag{10}$$

Here u and d represent a global dependence to account for the fact that these processes rely in some way on the diffusion of different molecules through large areas of tissue, for which $\kappa(t)$ is taken as a proxy (Klintsova & Greenough, 1999). The local probabilities π and η introduce a dependence on the local properties of the network. Each time a node i is selected according to Eq. (10), a second node j is then randomly chosen to be connected to

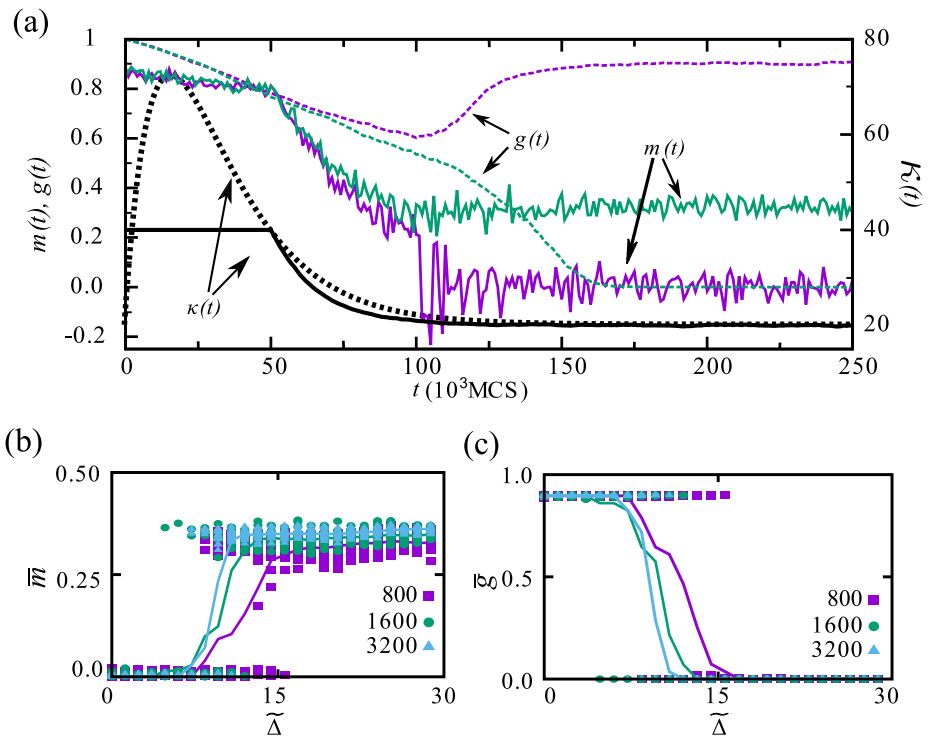

Fig. 1. (a) The black lines represent $\kappa(t)$ as given by the realistic model (black dashed line) and the linear approximation model (black solid line). The coloured lines show two exemplary temporal evolutions of the linear model. We represent $m(t)$ (coloured solid lines) and $g(t)$ (coloured dashed lines) for two realizations leading to two qualitatively different steady states, implying multistability in the system. In green, a series in which the network keeps memory and heterogeneity in the steady state. In purple, the opposite example. All parameters are the same in both situations ($N = 1600$, $n = 3$, $\kappa_0 = 40$ and $\kappa_\infty = 20$ and $\Delta = 5 \cdot 10^4 MCS$). MCS stands for Monte Carlo Steps. (b) $\bar{m}(\widetilde{\Delta})$ and (c) $\bar{g}(\widetilde{\Delta})$ curves for different system sizes, where $\widetilde{\Delta} = \Delta/\tau_p$. Results are for $\kappa_0 = 40$ and $\kappa_\infty = 20$. The parameter n is scaled with the network size, so that $n = 5, 10, 20$ respectively for $N = 800, 1600, 3200$. (For interpretation of the references to colour in this figure legend, the reader is referred to the web version of this article.)

(or disconnected from) i. Thus, two processes can lead to an increase (decrease) in a node degree, and we define the effective probabilities $\widetilde{\pi}$ and $\widetilde{\eta}$ to account for this.

Provided that $\widetilde{\pi}(I_i)$ and $\widetilde{\eta}(I_i)$ are normalized over the network, the evolution of $\kappa(t)$ only depends on $u(\kappa)$ and $d(\kappa)$, according to (Huttenlocher & Dabholkar, 1997; Johnson, Marro et al., 2010; Millán, Torres, Johnson et al., 2018; Millán, Torres, Marro, 2019; Navlakha et al., 2015)

$$\frac{d\kappa(t)}{dt} = 2\left[u\left[\kappa(t)\right] - d\left[\kappa(t)\right]\right]. \tag{11}$$

The factor 2 comes from the fact that the network is undirected, so each time a link is added or removed, it affects the degree of two nodes. Therefore, the evolution of the mean connectivity in the network only depends on the global probabilities, whereas the local probabilities characterize which nodes gain and lose links. The exponential decay of the connectivity caused by synaptic pruning can be modelled by u and d as

$$\begin{aligned} u(\kappa) &= \tfrac{n}{N}\left(1 - \tfrac{\kappa}{2\kappa_\infty}\right) \\ d(\kappa) &= \tfrac{n}{N}\tfrac{\kappa}{2\kappa_\infty}. \end{aligned} \tag{12}$$

where κ_∞ is the stationary mean connectivity, and n/N characterizes the speed of synaptic growth and death. Considering an initial configuration with $\kappa_0 = \kappa(t=0) > \kappa_\infty$, these lead to

$$\kappa(t) = (\kappa_0 - \kappa_\infty)\exp\left(-t/\tau_p\right) + \kappa_\infty, \tag{13}$$

where $\tau_p = N\kappa_\infty/(2n)$ sets the temporal scale of the pruning process. With this definition, $\kappa(t)$ decays exponentially from κ_0 to κ_∞.

Experimental evidence indicates a fast growth of the synaptic density following birth and preceding synaptic pruning, whose impact on brain development is yet to be fully clarified (Navlakha et al., 2015; Sayama et al., 2014). These profiles of synaptic density during infancy can be reproduced by considering an initial, fast growth of synapses followed by synaptic pruning (Millán, Torres, Johnson et al., 2018; Millán, Torres, Marro, 2019), namely

$$\begin{aligned} u(\kappa) &= \tfrac{n}{N}\left[1 - \tfrac{\kappa}{2\kappa_\infty} + a_g \exp(-t/\tau_g)\right] \\ d(\kappa) &= \tfrac{n}{N}\tfrac{\kappa}{2\kappa_\infty}, \end{aligned} \tag{14}$$

where τ_g and a_g control the time-scale and intensity of the initial growth. According to Eq. (14), the evolution of the mean connectivity is given by

$$\kappa(t) = \kappa_\infty\left[1 - b\exp(-t/\tau_g) + c\exp(-t/\tau_p)\right], \tag{15}$$

where $b = a_g\tau_g\left(\tau_p - \tau_g\right)^{-1}$ and $c = \kappa_0/\kappa_\infty + b - 1$. This model for $\kappa(t)$ (dashed black line in Fig. 1a) has been shown to reproduce experimental data of the mean synaptic density in the cortex in humans and rodents (Millán, Torres, Johnson et al., 2018).

The mean synaptic density $\kappa(t)$ as given by Eq. (15) presents a maximum $\kappa^* = \kappa(t^*)$ at

$$t^* = \frac{\tau_g\tau_p}{\tau_p - \tau_g}\ln\left(\frac{\tau_p b}{\tau_g c}\right). \tag{16}$$

Both t^* and κ^* depend non-trivially on a_g, τ_g and τ_p. In order to reduce the dimensionality of the model and study the effect of the non-trivial transient of high connectivity on the emergent state of the system in a systematic manner, here we consider a first order approximation to this realistic pruning profile. In particular, $\kappa(t)$ is kept constant (and high), $\kappa(t) = \kappa_0$, at the onset of the evolution, during a "fixed-density" time Δ, by imposing that the

same number of links are created and destroyed at each time step, namely

$$u(t) = d(t) = d_0 \ \forall t < \Delta, \tag{17}$$

where $d_0 = const$, and in particular we consider here $d_0 = n/N$. Thereafter, the mean degree is allowed to vary following the pruning dynamics given by Eq. (12). This allows us to easily control the width (Δ) and height ($\kappa^* = \max(\kappa_t)$) of the pruning process, which fully characterize it. An example of the evolution of $\kappa(t)$ for this model is shown in Fig. 1a (solid black line).

2.3. Local network structure

The local probabilities $\widetilde{\pi}$ and $\widetilde{\eta}$ introduce a dependence on the activity state of the neurons, and account for local heterogeneity. Following previous studies, we take

$$\begin{array}{lll} \widetilde{\pi}(I_i) & \propto & I_i^{\alpha}, \quad \alpha > 0 \\ \widetilde{\eta}(I_i) & \propto & I_i, \end{array} \tag{18}$$

which corresponds to synapses being chosen at random for removal, which can be seen as a first order approximation of pruning dynamics (Johnson et al., 2009). These definitions characterize the coupling between neural activity and structure. However, the particular functions are an arbitrary choice and other ones could be considered (Millán, Torres, Johnson et al., 2018; Millán, Torres, Marro, 2019). In this scenario, the parameter α characterizes the dependence on the local current.

Thus, α is the control parameter characterizing the emerging structure of the network: depending on α, nodes with high incoming current will be more likely to either gain ($\alpha > 1$) or lose ($\alpha < 1$) links. As shown in previous works (Johnson, Marro et al., 2010; Millán, Torres, Johnson et al., 2018), if the network is on a memory state ($m > 0$), then I_i is strongly correlated to the node degree k_i through the overlap $m(t)$. Therefore, for high α, high degree nodes will continue to gain new links as the network evolves, resulting in the appearance of hubs and a heterogeneous network structure. However, this is only the case if the system is in a memory state. If, on the contrary, neuronal dynamics is governed by noise, then I_i is randomly distributed and uncorrelated to k_i, given that the overlap $m(t)$ is also randomly distributed around 0. Eventually, this results in random rewiring of the links and leads to a homogeneous network with all nodes having similar, low degrees.

Thus, in this context network structure can be characterized by its degree distribution $p(k, t)$ characterizing the probability that a node has degree k at time t. This can be described by the homogeneity parameter $g(t)$ (Barrat et al., 2008; Johnson, Marro et al., 2010; Millán, Torres, Johnson et al., 2018),

$$g(t) = \exp\left(-\sigma_k^2(t)/\kappa(t)\right), \tag{19}$$

where $\sigma_k^2(t)$ is the variance of the degrees of the nodes. $g(t)$ equals 1 if $p(k) = \delta_{k_0,k}$, corresponding to a completely homogeneous degree distribution, i.e. one in which all nodes are homogeneous and have the same degree. On the contrary, $g(t)$ tends to 0 for networks with highly heterogeneous degree distributions. An extreme case is a bimodal degree distribution, that is, one with two maxima indicating the emergence of two types of nodes, one with low and another with high degree. This describes a star-like network in which a few hubs (nodes with high degree) are connected to the rest of the nodes in the network, which have low degree. Another example of a heterogeneous degree distribution is a scale-free one, that is, a network whose degree distribution is power-law distributed, such that all degrees have non-zero probability to occur in the network. In the following, we refer to networks with homogeneous (heterogeneous) degree distributions simply as homogeneous (heterogeneous) networks (Barrat et al., 2008). In the "topological limit" of this model ($I_i \to k_i$), the stationary value $\bar{g} \equiv g(t \to \infty)$ undergoes a continuous phase transition from homogeneous networks to heterogeneous ones at $\alpha_c = 1$ (Johnson, Marro et al., 2010).

Table 1
Model parameters. We indicate here the values of the model parameters used in the main text. N is the number of nodes (neurons) in the network; T is the noise parameter of the neuronal dynamics, or *temperature* $a_0 = \langle s_i^p \rangle$ is the mean activation of the stored memory pattern; n the parameter setting the rate of synaptic turnover (Eq. (14)); α is the pruning parameter controlling the scaling of the nodes' probability to gain a link; $\kappa_i nty$ is the stationary mean degree (or connectivity) in the network; and h_s is the number of MCS that the neuronal dynamics is updated between each network change.

Parameter	N	T	a_0	n	α	κ_∞	h_s
Value	1600	1.30	0.5	3	1.20	20	10

2.4. Monte Carlo simulations

The initial conditions for the neuronal states are randomly selected (prob $(s_i = 1) = 0.5$ initially). Network topology is initially given by an Erdős–Rényi network with given mean connectivity κ_0 (Erdős & Rényi, 1960; Molloy & Reed, 1995). This is a homogeneous configuration with $p(k, 0) = \delta_{\kappa_0,k}$ and $g(t = 0) \to 1$.

Time evolution is then accomplished by using the BKL algorithm as follows Millán, Torres, Johnson et al. (2018). At each time step, the number of links to be added and removed is selected according to two Poissonian distributions with means $Nu(\kappa)$ and $Nd(\kappa)$ (if $t > \Delta$) or Nd_0 (if $t \leq \Delta$). Then, as many times as necessary according to this draw, we select a node i with probability $\pi(I_i)$ to be assigned a new link to a node j chosen with random uniform probability $1/N$ (neglecting correlations). Similarly, we choose a new node i' according to $\eta(I_{i'})$ to lose a link to a node j', also chosen with random uniform probability $1/k_{i'}$. Therefore, the effective values of the local probabilities are explicitly given by

$$\begin{array}{lll} \widetilde{\pi}(I_i) & = & \frac{1}{2}\left(\pi(I_i) + \frac{1}{N}\right) \\ \widetilde{\eta}(I_i) & = & \frac{1}{2}\left(\eta(I_i) + \frac{k_i}{\kappa N}\right), \end{array} \tag{20}$$

where the 1/2 factor has been included to ensure normalization. Thus, according to the definition of $\widetilde{\pi}$ and $\widetilde{\eta}$, one has

$$\begin{array}{lll} \pi(I_i) & = & \max\left(2\frac{I_i^{\alpha}}{\langle I^{\alpha}\rangle N} - \frac{1}{N}\right), \\ \eta(I_i, k_i) & = & \max\left(2\frac{I_i}{\langle I\rangle N} - \frac{k_i}{\kappa N}\right), \end{array} \tag{21}$$

where normalization of π, η, $\widetilde{\pi}$, $\widetilde{\eta}$ has been imposed. Note that, due to the undirected nature of the network, links that are added and removed are bidirectional, so both the incoming and outgoing connections are (equally) changed.

The time scale for structure changes is set by the parameter n, whereas the time scale of the neuronal dynamics is measured in terms of Monte Carlo Steps (MCS). Each MCS consists on the actualization of N randomly chosen neurons (i.e. according to *Glauber dynamics* Amit, 1989). In particular, the system undergoes h_s MCS of the neuronal dynamics between each structural network update. Previous studies show a low dependence on this parameter in the cases of interest, so we report results here for $h_s = 10$ MCS (Millán, Torres, Johnson et al., 2018; Millán, Torres, Marro, 2019).

In this work, we used system sizes $N = 800$, 1600 and 3200, for Section 3.1, and $N = 1600$ in the rest. The sample size for each result was chosen by convergence of the mean value. A summary of the values of the parameters used in the text (except for Section 3.1) is shown in Table 1. Measures of the global variables on the stationary state are obtained by averaging during a long window of time: $\bar{f} = \Delta t^{-1} \sum_{t=t_0}^{t_0+\Delta t} f(t)$.

3. Results

The model that we have presented couples the form (as given by the underlying network structure) and function (as given by the neuronal dynamics) of the developing system. Under this coupled dynamics, the macroscopic state of the system depends on the level of thermal and topological noise, respectively characterized by the temperature T, and the structural parameter α. Previous work has characterized the phase diagram of the system with respect to these two parameters on a network undergoing synaptic pruning ($a_g = 0$ in Eq. (14)) (Millán, Torres, Johnson et al., 2018; Millán, Torres, Marro, 2019). In particular, three phases were shown to appear, depending on parameters: *(i)* a phase in which the network is homogeneous and displays memory (*homogeneous memory* phase) when both α and T are low; *(ii)* a phase in which the network is bimodal (appearance of hubs) and displays memory (*heterogeneous memory* phase) for high α and bounded T; and *(iii)* a phase in which the dynamics is governed by noise and therefore networks are homogeneous and do not display memory (*homogeneous noisy* phase) for high very T and bounded α.

The transition between the heterogeneous memory and homogeneous noisy phases was shown to take place through a bistability region corresponding to moderate α values, $1 < \alpha < 2$, and high temperature, $T > 1$. The bistability is a direct consequence of the coupling between form and function, and ultimately due to the emergence of hubs in heterogeneous networks that stabilize the memories. In fact, due to the presence of hubs, heterogeneous networks are more tolerant to thermal noise than homogeneous ones, and the critical temperature T_c separating the memory and non-memory phases effectively diverges from $T_c = 1$ for homogeneous networks to $T_c \to \infty$ for heterogeneous ones (de Franciscis et al., 2011; Torres et al., 2004). In this region, the stationary state of the system depends on its initial configuration: networks that are initially heterogeneous display memory and enhanced heterogeneity during the evolution of the system, whereas homogeneous ones fall into the noisy state.

Consequently, adding the initial overgrowth of synapses observed experimentally could have important consequences on the emerging behaviour of the system in this bistability region, as it would change the configuration of the system before synaptic pruning begins, possibly altering its subsequent development as well. Therefore, in the following we analyse the effect of the non-trivial transient of high connectivity preceding synaptic pruning on the dynamics of the system on the bistability region. In particular, we consider the point $\alpha = 1.2$, $T = 1.3$.

3.1. Emerging behaviour

An example of the evolution of our system is shown in Fig. 1a. The initial *fixed-density* period ($t < \Delta$) provides a non-trivial transient of network evolution during which links are added and removed but $\kappa(t)$ is kept constant and equal to κ_0. Even though $T > 1$, if κ_0 is sufficiently large, the system can retrieve the stored pattern throughout this period, as indicated by an overlap $m(t)$ significantly different from zero. Given that the topological dynamics is also taking place, there is meanwhile an underlying rewiring process that changes the underlying network structure. And, given that $\alpha > 1$ and the system is in a memory state, high degree nodes are more likely to gain new links. Eventually, the network becomes more heterogeneous ($g(t)$ decreases) and hubs start to appear.

After a time Δ, synaptic pruning begins, and the connectivity starts decreasing. The system can then either fall into the noise state and lose its heterogeneity (purple lines in Fig. 1a), or remain in the heterogeneous memory state (green lines), showing multistability. If the system remains in the memory state, it continues to heterogenize ($g(t) \to 0$), to the point that it can maintain a memory state as $\kappa(t) \to \kappa_\infty$ (dashed green line in Fig. 1a). On the other hand, if the neural network falls into the noisy state ($m(t) \approx 0$), neural activity – and hence synaptic growth and death – become uncorrelated with node degree, and the topology reverts gradually to a more homogeneous configuration ($g(t) \to 1$, dashed purple line), incapable of memory retrieval.

In general, for a given κ_0 there is a discontinuous phase transition as Δ is increased from the homogeneous noisy phase with $\bar{m} \to 0$ and $\bar{g} \to 1$ to the heterogeneous memory phase, with $\bar{g} \to 0$ and $\bar{m} > 0$, as shown respectively in panels (b) and (c) of Fig. 1 (where Δ has been re-scaled as $\widetilde{\Delta} = \Delta/\tau_p$). A finite size analysis shows that the results hold for increasing network size (Fig. 1b,c is for $N = 800$, 1600 and 3200). Therefore, in the following we restrict ourselves to the case $N = 1600$, which allows faster simulations than $N = 3200$ whilst the phase transition is not strongly affected. According to this finite-size analysis, we expect that the results hold for increasing sizes with an appropriate re-scaling of the model parameters. In order to characterize the stationary properties of the system, we define p_U as the probability that a given realization of the system ends in the heterogeneous memory state, for a given set of parameters.

3.2. Non-linear effect of the initial density

The initial density κ_0 also has a major effect on the dynamics, determining whether the system will be able to maintain memory retrieval and the minimum time $\widetilde{\Delta}$ in the high-density state necessary for it. In order to visualize this, we analyse the curves $p_U(\widetilde{\Delta})$ for different values of κ_0 in Fig. 2(a).

In the case $\kappa_0 = \kappa_\infty$, $\kappa(t)$ is trivially constant during the evolution of the system and, given that $T > 1$, the system falls into the noisy state regardless of $\widetilde{\Delta}$, so that $p_U \to 0$ for any value of $\widetilde{\Delta}$, (see $\kappa_0 = 20$ in Fig. 2a). However, even with a small increase in the synaptic density ($\kappa_0 = 25$), the memory state can be reached even for very low $\widetilde{\Delta}$ and $p_U \to 1$ as $\widetilde{\Delta}$ increases.

One might expect that the memory state would become easier to reach with higher κ_0 but, in fact, the opposite effect is obtained, and networks with increasing κ_0 take longer $\widetilde{\Delta}$ to reach the heterogeneous memory phase, for $\kappa_0 \gg \kappa_\infty$. This is illustrated in Fig. 2(c), where the complementary representation $p_U(\kappa_0)$, for fixed values of $\widetilde{\Delta}$, is shown. Up to very large values of $\widetilde{\Delta}$, the curves present a maximum for intermediate connectivities, indicating that for these values the system is more likely to reach the heterogeneous memory state.

This apparent paradox is explained after a deeper look at the system. In fact, large κ_0 implies that networks are initially more homogeneous due to the finite network size. This is because, in heterogeneous networks, the majority of the connections belong to the hubs. If the connectivity increases, more hubs appear, which are connected to most nodes in the network. This, in turn, limits the minimum degree of the low-degree nodes, since they are connected to the hubs (Barabási, 2016; Barrat et al., 2008). Besides, more links have to be pruned to make a significant change in the network, which slows down network evolution. In consequence, densely connected networks are more likely to fall into the noise state for a given $\widetilde{\Delta}$.

3.3. Robustness of the results

The previous results consider a fixed number d_0 (as defined in Eq. (17)) of rewired links during the initial high-density transient, for all values of κ_0. One may argue, however, that the rate of synaptic turnover should depend on the number of existing synapses, that is, $d_0 = f(\kappa_0)$. In order to estimate this relation, we calculate the mean number d_m of links added and removed

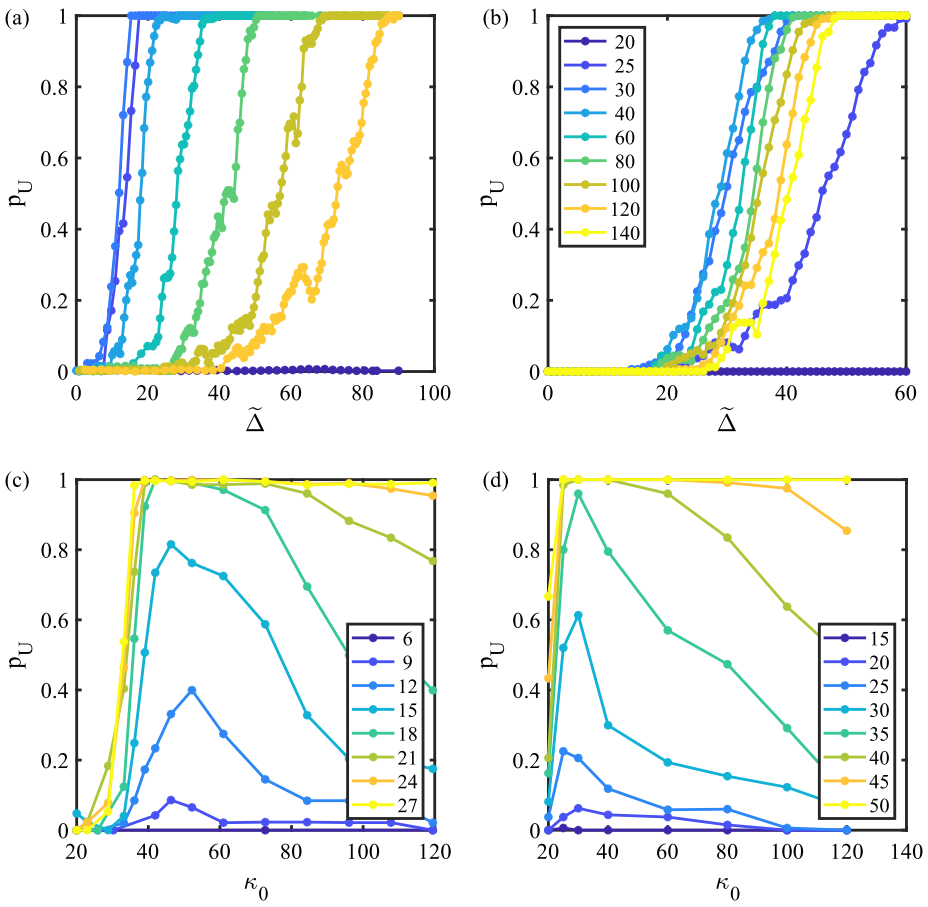

Fig. 2. Fraction of realizations that reach the heterogeneous memory state, or up state, p_U, respectively for models A (panels *a* and *c*) and B (panels *b* and *d*). (a, b) p_U is shown as function of $\widetilde{\Delta}$ and for different values of κ_0 as indicated in the legend in panel *b*. (c, d) p_U as function of κ_0 for different values of $\widetilde{\Delta}$ as indicated in the legend. $N = 1600$ and other parameter values as in Fig. 1. $\widetilde{\Delta}$ for model B is defined as $\widetilde{\Delta} = \Delta/1000$.

in the realistic model between the two times t_1 and t_2 such that $\kappa(t_1) = \kappa(t_2) = \kappa_0$, $t_1 < t_2$. Namely,

$$d_m \equiv \frac{1}{t_2 - t_1} \sum_{t=t_1}^{t_2} d(\kappa(t)). \tag{22}$$

Thus, d_m gives the average rate of synaptic turnover during the maximum of high connectivity. A parabolic approximation of $\kappa(t)$ (as given by Eq. (15)) around κ^* gives for d_m

$$d_m \approx d_m^p \equiv \frac{1}{4\tau_p}\left(\kappa^* + \frac{1}{6} D \Delta_\kappa^2 \kappa_\infty\right), \tag{23}$$

where $D = \tau_g^{-2}\left(\kappa^*/\kappa_\infty - 1\right) - c\left(\tau_g^{-2} - \tau_p^{-2}\right) e^{-t^*/\tau_p}$ and $\Delta_\kappa = \kappa^* - \kappa_0$. Numerical analysis indicates that the error associated with the parabolic approximation is less than 5%.

Eq. (23) suggests the scaling relation $d_0 \propto \kappa_0$, and in particular we consider here $d_0 = n\kappa_0/(\kappa_\infty N)$, such that the number of links rewired at each time depends linearly on κ_0. Note that this is the same dependence as introduced by the pruning rate in (12). In the following, we refer to this definition as model B and to the former with $d_0 = n/N$ as model A. We show the corresponding phase transition curves for model B in Fig. 2(b, d). These indicate that the main results also hold with model B, as there is also an optimal intermediate value of κ_0 that requires a minimum time Δ to achieve memory retrieval in the stationary state. Thus, there is a non-linear effect of the initial density on the emerging behaviour of the system.

3.4. Optimal transient connectivity

As shown in panels (*b*) and (*d*) of Fig. 2, respectively for models A and B, $p_U(\kappa_0)$ for a given $\widetilde{\Delta}$ shows a bell shape with a maximum for moderate κ_0, corresponding to $\kappa_0^A \approx 27$ and $\kappa_0^B \approx 40$ respectively for models A and B. More generally, one can measure the time needed by the model in the high-density state to ensure a given percentage of memory recovery in the stationary state. In particular, we define $\widetilde{\Delta}^a_{\min}(\kappa_0)$ as the minimum value of $\widetilde{\Delta}$ needed to reach an average stationary mean overlap equal to $m_a = 0.1a\ \bar{m}$, $a = 1, 2, \ldots, 10$, for a given κ_0. Minimal values of $\widetilde{\Delta}^a_{\min}$ indicate that lesser times are needed in the high-density state so as to reach memory with a minimal energy consumption. Our measures (Fig. 3(a), (b)) indicate a minimum $\widetilde{\Delta}^a_{\min}$ coincidently with κ_0^A and κ_0^B, in each model description. Therefore, memory is not only reached faster but it is also stronger for the optimal κ_0.

Finally, an integrated view of the effect of network dynamics and the emergent behaviour of the system can be obtained by the phase diagram of the system (Fig. 4(c), (d)) representing $\bar{m}(\widetilde{\Delta}, \kappa_0)$. High values (yellow areas) indicate the heterogeneous memory phase, whereas the homogeneous noisy phase appears as low values (blue areas) of $\bar{m}$. The phase transition between the two phases moves to higher $\widetilde{\Delta}$ for higher κ_0 in an approximately linear manner, as previously discussed, leading to the contraction of the heterogeneous memory region for high κ_0. On the other hand, very small κ_0 never leads to memory, due to the high thermal noise.

Summing up, our results show the benefit of intermediate densities with respect to very high ones during the transient

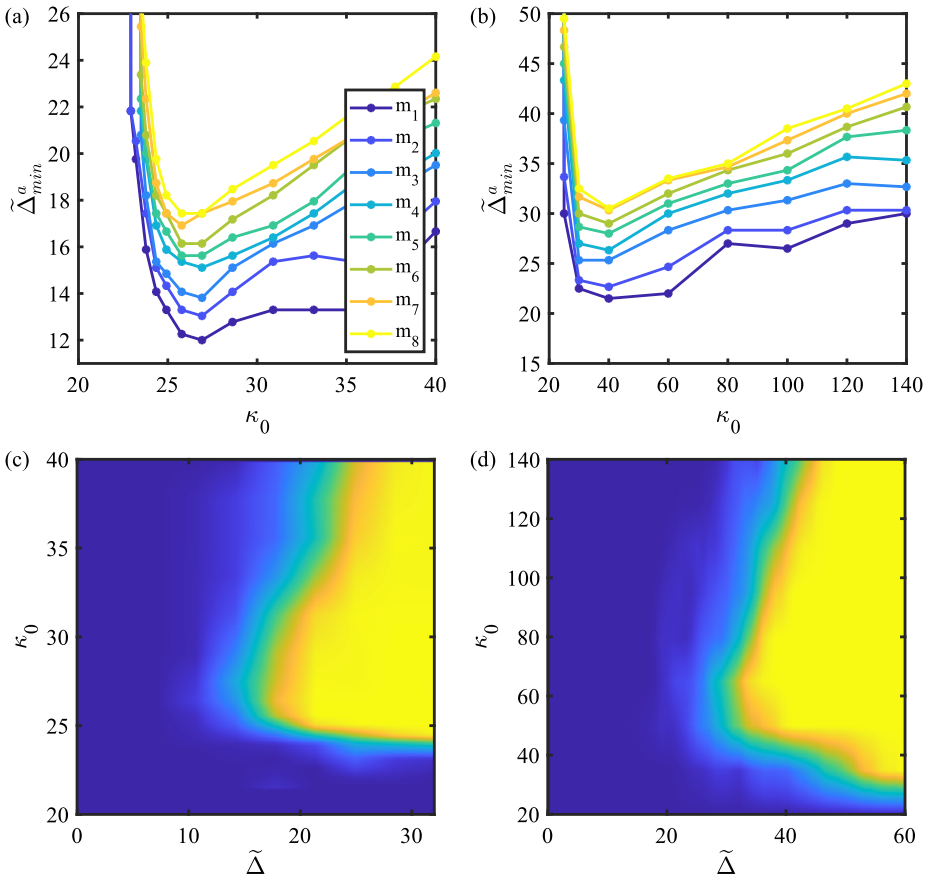

Fig. 3. Panels (a) and (b) show $\widetilde{\Delta}^a_{min}(\kappa_0)$ for $a = 1, \ldots, 8$ as indicated by m_a in the legend, respectively for models A and B. Panels (c) and (d) show the two dimensional phase diagram of the system, respectively for models A and B, indicated by $\bar{m}(\widetilde{\Delta}, \kappa_0)$. The homogeneous noisy phase appears as low memory values (blue region), whereas the heterogeneous memory one appears as high values (yellow region). Parameter values as in Fig. 2. (For interpretation of the references to colour in this figure legend, the reader is referred to the web version of this article.)

development of the network in order to achieve memory in a noisy environment. Interestingly, results hold when the density of synaptic turnover d_0 is re-scaled linearly with the density of synapses κ_0, indicating that the change in time scale is stronger than linear. Thus, the longer transient time needed to reach the heterogeneous memory phase for higher κ_0 is not only due to the higher number of synapses that need to be rewired. This result suggests that, for an evolving network such as the infant brain, it would be detrimental to initially grow a very high density of synapses, since this increases the energy costs during growth and also during the pruning process, and it does not improve memory retrieval or network structure. On the contrary, a neural network with intermediate values of transient synaptic density would perform more efficiently during pruning. We note that these results refer to the maximum synaptic density reached during infancy relative to the stationary value in the adult brain. High densities in general are known to lead to higher tolerance to noise (Amit, 1989; Millán, Torres, Marro, 2019) and also higher memory storage capacity (Knoblauch et al., 2014).

3.5. Transient heterogeneity determines memory stability.

The previous analysis has shown a quadratic dependence of the stationary state on κ_0 (see Fig. 3), and the emergence of multistability for intermediate values. However, the question remains of what determines, on a given trial, the stationary state of the system. Based on the results shown above, we propose that it is the transient level of heterogeneity (that is, the heterogeneity at the onset of the pruning) which determines the probability that the network will maintain memory.

In order to explore this hypothesis, we first define g_Δ and m_Δ as the values of $g(t)$ and $m(t)$ at the beginning of the pruning, that is, $g_\Delta = g(t = \Delta)$ and $m_\Delta = |m(t = \Delta)|$. These definitions allow us to explore how the stationary state depends on the transient evolution of the system. In Fig. 4(a), (b) we show the probability p_U that the system reaches the heterogeneous memory state as a function of g_Δ. This indicates a continuous transition from the heterogeneous memory state to the homogeneous noisy one as g_Δ increases. Moreover, there is a collapse of the curves for different κ_0. In consequence, g_Δ determines whether the network will be able to maintain memory once the pruning begins: high onset heterogeneity (small g_Δ) implies stationary memory, whereas low heterogeneity (high g_Δ) implies a stationary noisy state. These results are independent of κ_0 and of the model used, indicating that g_Δ is a strong indicator of stationary memory.

What is the memory state that leads to this configuration? In Fig. 4(c), (d) we show p_U as a function of m_Δ. Since m_Δ does not unequivocally determine the stationary state, the curves do not collapse in this case. What is obtained instead is a bell-shape dependence, indicating an optimal development process for moderate values of the transient memory. These correlate with minimum values of g_Δ, so that the value of $\widetilde{\Delta}^a_{\min}$ necessary for a stationary memory state is also minimal for this value. In this sense, if $m_\Delta \ll 1$, there is no transient memory because κ_0 is too small and the network cannot display memory initially, thus remaining in a homogeneous configuration. On the other hand, if $m_\Delta \approx 1$, this is so because κ_0 is large and the network is still very homogeneous when pruning begins. In both cases, the network evolves towards a homogeneous configuration. Note that

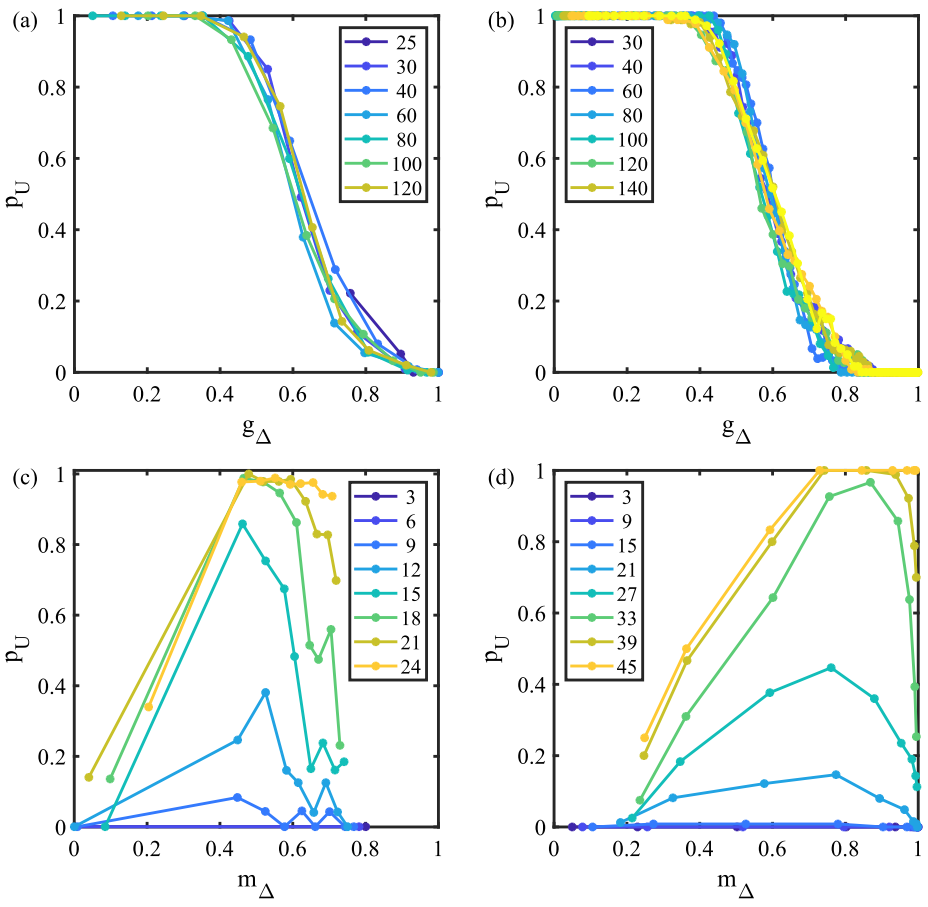

Fig. 4. Panels (a) and (b) show $p_U(g_\Delta)$, with different colours for different values of κ_0, as indicated by the legend, respectively for models A and B. Panels (c) and (d) show $p_U(m_\Delta)$, with different colours for different values of $\widetilde{\Delta}$, respectively for models A and B. (For interpretation of the references to colour in this figure legend, the reader is referred to the web version of this article.)

this qualitative result does not depend on the particular definition of d_0 since it holds for both models A and B.

4. Discussion

We have presented here an adaptive network model inspired by synaptic pruning that creates a dependence of the final network structure and memory state on the transient synaptic density, as one should probably expect in nature. In this model, the introduction of a high fixed-density transient allows for network heterogenization and for the settlement of a memory state under noisy conditions. We have analysed in detail a point of the phase space corresponding to a bistability area between two phases. These are a heterogeneous memory phase, in which the resulting networks have a heterogeneous structure and are capable of memory retrieval, and a homogeneous noisy one, in which the resulting networks are homogeneous and incapable of memory retrieval. In this region of the phase space, the system is most sensitive to the details of the evolution and the initial conditions. This happens to correspond to high T – the parameter characterizing the thermal noise in the neuronal dynamics (Eq. (3)) – so that the stability of the memory states is reduced, and also to large α – the parameter characterizing the scaling of the probabilities that each node gains or loses a link (Eq. (20)) —, so that the system can heterogenize. The selection of these model parameters has not been arbitrary, as the presence of a bistability region leads to increase sensibility to changes in the initial conditions. However, the qualitative results reported in this study would hold for different values of T and α as long as they fall within the bistability region.

In these conditions, we have found that the model exhibits a discontinuous (first order) phase transition as one varies the length of the transient period of fixed density, $\widetilde{\Delta}$, and the value of this density, κ_0. In fact, there is a quadratic effect of κ_0, such that intermediate values provide a faster and more stable evolution towards a memory stationary state, and there is an optimal κ_0 that optimizes the evolution into such a state. We have also shown that the transient heterogeneity determines the stationary state of the system. Given the aforementioned feedback loop, this depends on the transient memory m_Δ and κ_0, so that the stationary state of the system is ultimately determined by its physiological history.

4.1. Implications for brain development

These results shed light on why brain development would occur through the initial creation of a great many synapses which are then gradually pruned. If the final density is optimal for energy consumption, why should one go through a transient state of twice this density? Our neural network with an evolving structure based on some simple biological considerations shows that the eventual memory stability on the system does indeed depend on whether it passed through a transient period of relatively high synaptic density. A feedback loop thus emerges between neural activity and network topology such that, beginning with a random network, a transient state of high density can allow for the subsequent pruning of synapses as the topology is optimized for the particular learnt memories (Knoblauch et al., 2014; Knoblauch & Sommer, 2016). This goes in line with previous studies indicating that a higher synaptic density – as occurs during infancy –

allows for faster learning, which might be key during development (Knoblauch et al., 2014; Knoblauch & Sommer, 2016). Thus, a larger synaptic density during infancy would serve to increase both the storage capacity and the stability against noise of the eventual adult network.

What limits the maximum synaptic density then? An even higher density would allow for faster learning and increased storage capacity during infancy (Knoblauch et al., 2014; Knoblauch, Palm, & Sommer, 2010; Knoblauch & Sommer, 2016). However, experimental observations indicate that the maximum synaptic density during infancy is much smaller than what it could be reached if all possible synapses (taking into account geometrical and physiological constraints) existed (Chklovskii, Mel, & Svoboda, 2004; Stepanyants et al., 2002). Energy consumption considerations likely play a role on this bound, as not only more synapses would need to be maintained but also created and pruned. Our study points to another concurrent mechanism that would limit the maximum connectivity as further increases above a given value would not increase the stability of the memories against noise. Thus, our results could help explain why real world networks such as those in the brain do not create enormous numbers of synapses to begin with during early development, as this would increase the demand for resources, whilst not necessarily helping network development. It is important to note, however, that this result refers to the maximum connectivity reached during infancy relative to the stationary value in the adult brain. In general, for a given setting higher connectivities are known to increase the tolerance to noise (Amit, 1989) and also the memory storage capacity of the network (Knoblauch et al., 2014).

Why, though, should the brain not begin with both the low density – to minimize energy consumption – and high heterogeneity — for good memory stability? We conjecture that much less genetic information is needed to build a random neural network that is subsequently shaped by its dynamics (under the influence of actual environmental conditions), than to specify a particular structure. This would also be a more robust developmental path. Moreover, beginning with a moderately dense random graph may allow for greater plasticity, since the pruning mechanism will fashion a network well-adapted to the specific patterns stored (Knoblauch et al., 2014; Millán, Torres, Johnson et al., 2018).

4.2. Robustness of the results

We have analysed the robustness of the results to details of the model and the validity of the approximations considered. In particular, we have defined a more realistic approximation such that the rate of synaptic growth and death during the fixed high-density period is proportional to this connectivity. We have found that the qualitative behaviour of the system does not depend on these details. Namely, there is also a discontinuous transition from a homogeneous non-memory state to a heterogeneous memory one as the duration Δ of the transient period increases, whereas there is a non-linear dependence on κ_0, and the stationary state of the system is ultimately determined by g_Δ. Therefore, the results obtained in this work – i.e. the benefits of a transient high connectivity period, the second order effect of κ_0 and the crucial effect of g_Δ on the stationary state – are robust with respect to microscopic details of the pruning model.

It is important to note however that a number of simplifications and assumptions have been taken in the definition of the model. In fact, in this work we have coupled the simplest models able to produce the behaviours of interest, namely the associative memory property and a realistic pruning profile. Hebbian synaptic weights have thus been considered as a standard way to define memory attractors, which also introduces a dependence of the neuronal dynamics on the network topology (Amari, 1972; Amit, 1989; de Franciscis et al., 2011; Hebb, 2005; Hopfield, 1982; Morelli et al., 2004; Recio & Torres, 2016; Torres et al., 2004; Uhlig et al., 2013).

Similarly, we have only considered structural plasticity in this work. Consequently, the synaptic weights are defined ad-hoc and when a synapse is added into the network it already has the Hebbian weight given by Eq. (3). This amounts to considering an instantaneous learning process. There are, however, a few considerations that can support our assumption. Firstly, the memory states are stable with respect to the change of a few links, and the number of links changed at each step is much smaller than the number of links existing already in the network. Thus, it can be expected that the memory state would remain stable even with a different initialization of the weights. The weight values could then change following long-term weight plasticity, which occurs in faster time-scales than structural plasticity. Consequently, it can be assumed that the stabilization of the weights occurs on a faster time-scale than the network changes (Bi & Poo, 2001; Hebb, 2005; Klintsova & Greenough, 1999; Knoblauch & Sommer, 2016). Despite these considerations, synaptic pruning plays an important role in learning and, equivalently, learning also plays a fundamental role leading synaptic pruning (Knoblauch et al., 2014, 2010; Knoblauch & Sommer, 2016). It would thus be interesting for future works to include an explicit learning mechanism in the model to study the interplay of between network development and learning.

Furthermore, there is also an underlying symmetry between active and inactive neurons inherited from the canonical Amari–Hopfield model (Amit, 1989). In particular, this implies that inactive neurons (receiving a large negative local current) are as likely to gain new synapses as very active neurons (receiving a large positive current), and that the synapses connecting two silent neurons are as strong as those connecting two active neurons. These definitions are in line with a large number of previous studies on auto-associative memory model (Amari, 1972; Amit, 1989; de Franciscis et al., 2011; Hebb, 2005; Hopfield, 1982; Morelli et al., 2004; Recio & Torres, 2016; Torres et al., 2004; Uhlig et al., 2013), but it is however not likely the case for biological neuronal networks. More realistic situations could be implemented by small changes in the neuron model, such as considering different values of a_0 to break the symmetry between active and inactive states. Similarly, the memorized activity patterns could be modified to describe local states considering only a patch of active nodes, as other studies have done (Knoblauch et al., 2014; Knoblauch & Sommer, 2016). Different definitions of the learning rule and neuronal dynamics would change the details of the network structure, but we expect that our main results would hold, in accordance with previous studies (Millán, Torres, Johnson et al., 2018; Millán, Torres, Marro, 2019), and as long as the basic mechanism linking the neuronal and network states holds. Moreover, we showed in previous studies (Johnson, Marro et al., 2010; Millán, Torres, Johnson et al., 2018) that the generic features of our model also apply to the large scale configuration of the brain, and other biological networks such as protein interaction networks. Thus, the present situation could be applied to other systems, such as neuronal populations, in which the common deactivation of two populations can be actively enforced by a common inhibitory source, for instance.

Another assumption of the model is the consideration of an undirected symmetric network: $w_{ij} = w_{ji}$ and $e_{ij}(t) = e_{ji}(t)$ $\forall(i, j)$ and t, following previous studies (Johnson, Marro et al., 2010; Johnson et al., 2009; Millán, Torres, Johnson et al., 2018; Millán, Torres, Marro, 2019). The model could be easily generalized to include non-symmetric connections, either through the

definition of asymmetric weights, directed links, or both. In the current setting, we have considered symmetric Hebbian synapses as a standard way to define memory attractors, and therefore a useful tool to understand the effect of structural plasticity, and its coupling with memory, on network dynamics. More in general, symmetric connections are commonly used in the literature (Amit, 1989; de Franciscis et al., 2011; Hebb, 2005; Morelli et al., 2004; Recio & Torres, 2016; Torres et al., 2004; Uhlig et al., 2013) as they allow for analytic studies in terms of a Hamiltonian description. The introduction of asymmetry can lead to the emergence of chaos, for instance causing the system to oscillate among different states (Sompolinsky & Kanter, 1986), or other instabilities (Johnson, 2020). We expect that the main results of our studies would hold within reasonable definitions of asymmetry, as there are no indications to believe that the feedback between structure and dynamics would disappear when considering directed networks. This would be an interesting approach for future work.

Overall, the relation between the network structure – beyond the effect of the mean synaptic density – and its emerging memory characteristics are not dependent on most of the microscopic details. For instance, it is a well-known result that the critical point diverges for heterogeneous systems in which hubs are present (Barrat et al., 2008), explaining why the memory state remains stable even for high thermal noise levels in our model. Thus, more detailed models could be considered in general, with more biological plausibility, as well as modifications of the current model. These could be specifically tailored to reproduce specific characteristics of different systems, such as biological neuronal networks, large-scale brain networks, protein interaction networks or artificial neural networks. We expect that, as long as the basic ingredients of this model are maintained (i.e. the existence of a memory phase and a direct relation between the node's degree and local current), the interplay between structure and function, and the effect of different pruning profiles, will hold.

4.3. On the memory storage capacity

In this study we have considered how the temporal profile of synaptic pruning affects the stability of memory against thermal noise and the structural properties of the underlying network. Thus, for the sake of simplicity, we have only considered one stored memory pattern. In previous studies we showed that, when more patterns were stored in the network, the existing phases were maintained but new ones appeared corresponding to quenched (Millán, Torres, Johnson et al., 2018) and dynamical (Millán, Torres, Marro, 2019) memory states, depending on parameters. Analysing the interplay between different pruning profiles and the memory state on those phases would be an interesting starting point for new studies that could unravel new findings. We expect that the second order effect of the maximum synaptic density – relative to its stationary value in the adult brain – would still hold for higher memory loads. The actual optimal value of the synaptic density would depend on details of the model, number of stored patterns and rate of synaptic turnover. Future works should study this interplay in detail.

Similarly, characterizing the memory capacity of the model under these conditions, and how it is affected by different pruning profiles, would be an interesting addition to future studies. It is a well known result, for instance, that the capacity of a given network (as well as the stability of the memories against thermal noise) is higher for higher network densities, as we also showed explicitly for this model in previous works (Millán, Torres, Marro, 2019). However different pruning profiles can lead to different capacities during development and adulthood. It is worth noting, however, that the model presented here is not intended to optimize the network capacity, as in other studies (Knoblauch et al., 2010). Rather, our goal was to unravel the effect that different pruning profiles have on the development of the structural and memory properties of the network. For that, we have placed the system in a very suboptimal position with respect to memory retrieval, just in the interface between stable and unstable memories (Millán, Torres, Johnson et al., 2018), which is subjected to very strong thermal noise. This allows us to analyse the maximum effects of different pruning profiles.

4.4. Conclusion

We have presented a general model, whose main aspects are shared by different biological (such as protein interaction networks Albert, 2005; Berg et al., 2004; Millán, Torres, Johnson et al., 2018) and technical systems (Abiodun et al., 2018; Pagani & Aiello, 2013). Our work here may serve as a starting point and a very suitable theoretical framework for studying the relationship that may exist between certain neurological disorders that appear during brain development, such as childhood autism and schizophrenia in young adults, and different synaptic pruning profiles, as has recently been suggested (Afroz, Parato, Shen, & Smith, 2016; Sekar et al., 2016; Sayama et al., 2014). Moreover, it may also be of use to design new paradigms of artificial neural networks with technological applications.

Code availability

Generated codes are available from the corresponding author upon reasonable request.

CRediT authorship contribution statement

Ana P. Millán: Designed the model and the analyses, Wrote the original draft, Performed the formal analysis. **Joaquín J. Torres:** Designed the model and the analyses, Participated in the final manuscript. **Samuel Johnson:** Designed the model and the analyses, Participated in the final manuscript. **J. Marro:** Designed the model and the analyses, Participated in the final manuscript.

Declaration of competing interest

The authors declare that they have no known competing financial interests or personal relationships that could have appeared to influence the work reported in this paper.

Data availability

All data that support this study is available in the manuscript.

Acknowledgements

The authors acknowledge financial support from the Spanish Ministry of Science and Technology, and the Agencia Española de Investigación (AEI), Spain under grant FIS2017-84256-P (FEDER funds) and from the Consejería de Conocimiento, Investigación Universidad, Junta de Andalucía and European Regional Development Funds, Spain, Refs. SOMM17/6105/UGR and A-FQM-175-UGR18. APM also acknowledges support from "Obra Social La Caixa, Spain" (ID 100010434 with code LCF/BQ/ES15/10360004) and from ZonMw, Netherlands and the Dutch Epilepsy Foundation, Netherlands, project number 95105006. SJ acknowledges support from the Alan Turing Institute under EPSRC, United Kingdom Grant No. EP/N510129/1.

References

Abiodun, O. I., Jantan, A., Omolara, A. E., Dada, K. V., Mohamed, N. A., & Arshad, H. (2018). State-of-the-art in artificial neural network applications: A survey. *Heliyon*, *4*(11), Article e00938.

Achard, S., Salvador, R., Whitcher, B., Suckling, J., & Bullmore, E. (2006). A resilient, low-frequency, small-world human brain functional network with highly connected association cortical hubs. *Journal of Neuroscience*, *26*(1), 63–72.

Afroz, S., Parato, J., Shen, H., & Smith, S. S. (2016). Synaptic pruning in the female hippocampus is triggered at puberty by extrasynaptic GABAA receptors on dendritic spines. *Elife*, *5*, Article e15106.

Albert, R. (2005). Scale-free networks in cell biology. *Journal of Cell Science*, *118*(21), 4947–4957.

Amari, S. I. (1972). Characteristics of random nets of analog neuron-like elements. *IEEE Transactions on Systems, Man, and Cybernetics*, *2*, 643–657.

Amit, D. J. (1989). *Modeling Brain Function: the World of Attractor Neural Networks*. New York, NY, USA: Cambridge University Press.

Barabási, A. L. (2016). *Network Science*. Cambridge University Press.

Barabási, A. L., & Albert, R. (1999). Emergence of scaling in random networks. *Science*, *286*(5439), 509–512.

Barrat, A., Barthelemy, M., & Vespignani, A. (2008). *Dynamical processes on complex networks*. Cambridge university press.

Berg, J., Lässig, M., & Wagner, A. (2004). Structure and evolution of protein interaction networks: a statistical model for link dynamics and gene duplications. *BMC Evolutionary Biology*, *4*(1), 51.

Bi, G. Q., & Poo, M. M. (2001). Synaptic modification by correlated activity: Hebb's postulate revisited. *Annual Review of Neuroscience*, *24*(1), 139–166.

Bianconi, G., Darst, R. K., Iacovacci, J., & Fortunato, S. (2014). Triadic closure as a basic generating mechanism of communities in complex networks. *Physical Review E*, *90*(4), Article 042806.

Bianconi, G., & Rahmede, C. (2016). Network geometry with flavor: from complexity to quantum geometry. *Physical Review E*, *93*(3), Article 032315.

Boccaletti, S., Latora, V., Moreno, Y., Chavez, M., & Hwang, D.-U. (2006). Complex networks: structure and dynamics. *Physics Reports*, *424*(4–5), 175–308.

Bortz, A. B., Kalos, M. H., & Lebowitz, J. L. (1975). A new algorithm for Monte Carlo simulation of ising spin systems. *Journal of Computational Physics*, *17*(1), 10–18.

Chechik, G., Meilijson, I., & Ruppin, E. (1998). Synaptic pruning in development: a computational account. *Neural Computation*, *10*(7), 1759–1777.

Chechik, G., Meilijson, I., & Ruppin, E. (1999). Neuronal regulation: a mechanism for synaptic pruning during brain maturation. *Neural Computation*, *11*, 2061–2080.

Chklovskii, D. B., Mel, B. W., & Svoboda, K. (2004). Cortical rewiring and information storage. *Nature*, *431*(7010), 782.

Crossley, N. A., Mechelli, A., Scott, J., Carletti, F., Fox, P. T., McGuire, P., et al. (2014). The hubs of the human connectome are generally implicated in the anatomy of brain disorders. *Brain*, *137*(8), 2382–2395.

Eguíluz, V. M., Chialvo, D. R., Cecchi, G. A., Baliki, M., & Apkarian, A. V. (2005). Scale-free brain functional networks. *Physical Review Letters*, *94*(1), Article 018102.

Erdős, P., & Rényi, A. (1960). On the evolution of random graphs. *Publication of the Mathematical Institute of the Hungarian Academy of Sciences*, *5*(1), 17–60.

Faludi, G., & Mirnics, K. (2011). Synaptic changes in the brain of subjects with schizophrenia. *International Journal of Developmental Neuroscience*, *29*(3), 305–309.

de Franciscis, S., Johnson, S., & Torres, J. J. (2011). Enhancing neural-network performance via assortativity. *Physical Review E*, *83*(3), Article 036114.

Gastner, M. T., & Ódor, G. (2016). The topology of large open connectome networks for the human brain. *Scientific Reports*, *6*, 27249.

Gross, T., & Blasius, B. (2007). Adaptive coevolutionary networks: a review. *Journal of the Royal Society Interface*, *5*(20), 259–271. http://dx.doi.org/10.1098/rsif.2007.1229.

Hebb, D. O. (2005). *The Organization of Behavior. A Neuropsychological Theory*. Psychology Press.

Hopfield, J. J. (1982). Neural networks and physical systems with emergent collective computational abilities. *Proceedings of the National Academy of Sciences*, *79*(8), 2554–2558. http://dx.doi.org/10.1073/pnas.79.8.2554.

Huttenlocher, P. R., & Dabholkar, A. S. (1997). Regional differences in synaptogenesis in human cerebral cortex. *Journal of Comparative Neurology*, *387*(2), 167–178.

Iglesias, J., Eriksson, J., Grize, F., Tomassini, M., & Villa, A. E. (2005). Dynamics of pruning in simulated large-scale spiking neural networks. *Biosystems*, *79*(1–3), 11–20.

Johnson, S. (2020). Digraphs are different: Why directionality matters in complex systems. *Journal of Physics: Complexity*, *1*(1), Article 015003.

Johnson, S., Marro, J., & Torres, J. J. (2010). Evolving networks and the development of neural systems. *Journal of Statistical Mechanics: Theory and Experiment*, *2010*(03), P03003.

Johnson, S., Torres, J. J., & Marro, J. (2009). Nonlinear preferential rewiring in fixed-size networks as a diffusion process. *Physical Review E*, *79*(5), Article 050104.

Johnson, S., Torres, J. J., Marro, J., & Muñoz, M. A. (2010). Entropic origin of disassortativity in complex networks. *Physical Review Letters*, *104*(10), Article 108702.

Johnson, S., Torres, J. J., Marro, J., & Muñoz, M. A. (2011). Why are so many networks disassortative? In *AIP Conference Proceedings, Vol. 1332* (pp. 249–250). AIP.

Klintsova, A. Y., & Greenough, W. T. (1999). Synaptic plasticity in cortical systems. *Current Opinion in Neurobiology*, *9*(2), 203–208.

Knoblauch, A. (2017). Impact of structural plasticity on memory formation and decline. In *The Rewiring Brain* (pp. 361–386). Elsevier.

Knoblauch, A., Körner, E., Körner, U., & Sommer, F. T. (2014). Structural synaptic plasticity has high memory capacity and can explain graded amnesia, catastrophic forgetting, and the spacing effect. *PLoS One*, *9*(5), Article e96485.

Knoblauch, A., Palm, G., & Sommer, F. T. (2010). Memory capacities for synaptic and structural plasticity. *Neural Computation*, *22*(2), 289–341.

Knoblauch, A., & Sommer, F. T. (2016). Structural plasticity, effectual connectivity, and memory in cortex. *Frontiers in Neuroanatomy*, *10*, 63.

Marro, J., & Torres, J. J. (2021). *Phase transitions in grey matter: Brain architecture and mind dynamics*. Melville, New York: AIP Publishing (online), http://dx.doi.org/10.1063/9780735421769.

Maslov, S., & Sneppen, K. (2002). Specificity and stability in topology of protein networks. *Science*, *296*(5569), 910–913.

Millán, A. P., Gori, G., Battiston, F., Enss, T., & Defenu, N. (2021). Complex networks with tuneable spectral dimension as a universality playground. *Physical Review Research*, *3*(2), 023015.

Millán, A. P., Torres, J. J., & Bianconi, G. (2018). Complex network geometry and frustrated synchronization. *Scientific Reports*, *8*(9910).

Millán, A. P., Torres, J. J., & Bianconi, G. (2019). Synchronization in network geometries with finite spectral dimension. *Physical Review E*, *99*(2), Article 022307.

Millán, A. P., Torres, J. J., Johnson, S., & Marro, J. (2018). Concurrence of form and function in developing networks and its role in synaptic pruning. *Nature Communications*, *9*(1), 2236.

Millán, A. P., Torres, J., & Marro, J. (2019). How memory conforms to brain development. *Frontiers in Computational Neuroscience*, *13*.

Molloy, M., & Reed, B. (1995). A critical point for random graphs with a given degree sequence. *Random Structures & Algorithms*, *6*(2–3), 161–180.

Morelli, L. G., Abramson, G., & Kuperman, M. N. (2004). Associative memory on a small-world neural network. *The European Physical Journal B*, *38*(3), 495–500.

Navlakha, S., Barth, A. L., & Bar-Joseph, Z. (2015). Decreasing-rate pruning optimizes the construction of efficient and robust distributed networks. *PLoS Computational Biology*, *11*(7), 1–23.

Newman, M. E. J. (2003). The structure and function of complex networks. *SIAM Review*, *45*(2), 167–256.

Newman, M. (2018). *Networks*. Oxford University Press.

Ódor, G. (2013). Spectral analysis and slow spreading dynamics on complex networks. *Physical Review E*, *88*(3), Article 032109.

Ódor, G., & Hartmann, B. (2018). Heterogeneity effects in power grid network models. *Physical Review E*, *98*(2), Article 022305.

Pagani, G. A., & Aiello, M. (2013). The power grid as a complex network: a survey. *Physica A. Statistical Mechanics and its Applications*, *392*(11), 2688–2700.

Piraveenan, M., Prokopenko, M., & Zomaya, A. Y. (2008). Local assortativeness in scale-free networks. *EPL (Europhysics Letters)*, *84*(2), 28002.

Recio, I., & Torres, J. J. (2016). Emergence of low noise frustrated states in E/I balanced neural networks. *Neural Networks*, *84*, 91–101.

Sayama, H., Pestov, I., Schmidt, J., Bush, B. J., Wong, C., Yamanoi, J., et al. (2013). Modeling complex systems with adaptive networks. *Computers & Mathematics with Applications*, *65*(10), 1645–1664.

Schmidt, R., LaFleur, K. J., de Reus, M. A., van den Berg, L. H., & van den Heuvel, M. P. (2015). Kuramoto model simulation of neural hubs and dynamic synchrony in the human cerebral connectome. *BMC Neuroscience*, *16*(1), 54.

Sekar, A., Bialas, A. R., de Rivera, H., Davis, A., Hammond, T. R., Kamitaki, N., et al. (2016). Schizophrenia risk from complex variation of complement component 4. *Nature*, *530*, 177.

Sompolinsky, H., & Kanter, I. (1986). Temporal association in asymmetric neural networks. *Physical Review Letters*, *57*(22), 2861.

Stam, C. (2010). Characterization of anatomical and functional connectivity in the brain: a complex networks perspective. *International Journal of Psychophysiology*, *77*(3), 186–194.

Stepanyants, A., Hof, P. R., & Chklovskii, D. B. (2002). Geometry and structural plasticity of synaptic connectivity. *Neuron*, *34*(2), 275–288.

Su, G., Ruan, Z., Guan, S., & Liu, Z. (2013). Explosive synchronization on co-evolving networks. *EPL (Europhysics Letters)*, *103*(4), 48004.

Tang, G., Gudsnuk, K., Kuo, S.-H., Cotrina, M. L., Rosoklija, G., Sosunov, A., et al. (2014). Loss of mTOR-dependent macroautophagy causes autistic-like synaptic pruning deficits. *Neuron*, *83*(5), 1131–1143.

Torres, J. J., Muñoz, M. A., Marro, J., & Garrido, P. (2004). Influence of topology on the performance of a neural network. *Neurocomputing*, *58*, 229–234.

Uhlig, M., Levina, A., Geisel, T., & Herrmann, M. (2013). Critical dynamics in associative memory networks. *Frontiers in Computational Neuroscience*, *7*, 87.

Vazquez, F., Eguíluz, V. M., & San Miguel, M. (2008). Generic absorbing transition in coevolution dynamics. *Physical Review Letters*, *100*(10), Article 108702.

Watts, D. J., & Strogatz, S. H. (1998). Collective dynamics of "small-world" networks. *Nature*, *393*(6684), 440.

Wiedermann, M., Donges, J. F., Heitzig, J., Lucht, W., & Kurths, J. (2015). Macroscopic description of complex adaptive networks coevolving with dynamic node states. *Physical Review E*, *91*(5), Article 052801.